Two-temperature ablative material response model with application to Stardust and MSL atmospheric entries

H. Scandelli [a,b,*], A. Ahmadi-Senichault [a,b], J. Lachaud [a,c]

[a] I2M - Institute of Mechanical Engineering of Bordeaux: UMR CNRS 5295, University of Bordeaux, Arts et Métiers Institute of Technology, Hesam Université, Bordeaux INP, INRAE, 33400, Talence, France
[b] Arts et Métiers Institute of Technology, 33400, Talence, France
[c] Univ. Bordeaux, 33400, Talence, France

Keywords:
Local thermal non-equilibrium
Non-equilibrium chemistry
Thermal protection system
TACOT
Stardust and MSL missions

A B S T R A C T

Ablative material response codes currently in use consider local thermal equilibrium between the solid phases and the pyrolysis gases. For typical entry conditions, this hypothesis may be justified by the fact that the thermal Peclet number within the pores is small, which is a necessary condition for thermal equilibrium in non-reactive materials. However, the validity of this analysis may fall under some circumstances. The thermal Peclet number may become large due to high pyrolysis gas velocities. Additional physical phenomena not accounted for in the Peclet analysis may become non-negligible, such as the change of enthalpy due to chemical reactions. The objective of this study is two-fold. First, a detailed two temperature material response model for porous reactive materials is presented. This model has been implemented and made available in the Porous material Analysis Toolbox based on OpenFOAM (PATO). Second, the model is applied to the Theoretical Ablative Composite for Open Testing (TACOT) in a wide range of conditions to assess the true range of validity of the thermal equilibrium hypothesis. Simulations are carried out on the Stardust and Mars Science Laboratory (MSL) atmospheric entries. The main design variables have been monitored and compared between the two models: temperature evolution and species concentration within the material, pyrolysis gas blowing rate, extension of the pyrolysis zone, and wall recession due to ablation. Results show that under chemical equilibrium conditions, no significant deviation in the monitored quantities are observed, while under chemical non-equilibrium conditions there is a large impact on the species concentration.

1. Introduction

Extra-orbital missions often involve the analysis of entry processes into planetary atmospheres at hypersonic speeds. Under these conditions, a high enthalpy curved detached shock (bow shock) forms in front of the spacecraft and the kinetic energy is progressively dissipated into heat. Convection of this flow around the capsule and radiation progressively heat the material. The temperature at the surface of the material can increase to approximately 3000 K for severe entry conditions. To ensure the integrity of the structure, a thermal protection system (TPS) is designed to absorb and dissipate the heat through phase changes, chemical reactions, and material removal. Charring ablative materials represent a traditional approach to thermal protection [1–3]. A famous example is the new class of phenolic impregnated ablators (PICA [4], PICA-X, ASTERM [5]) that consists of a carbon fiber preform partially impregnated with phenolic resin, resulting in very light weight and excellent thermal insulation properties. When heated, the resin thermally decomposes and progressively carbonizes, losing mass and releasing pyrolysis gases. These gases percolate and diffuse towards the surface, reacting with each other (homogeneous reactions) and with the solid phases (heterogeneous reactions). Once at the surface, the gases are blown into the flow-field boundary layer, changing its composition. The blowing also induces a blockage of the convective heat flux impinging on the surface of the spacecraft, thus reducing the thermal load [6]. In addition, the surface of the heat shield is ablated due to the occurrence of heterogeneous chemical reactions between the boundary layer gases and the surface (oxidation, nitridation) and due to sublimation above 2500 K.

Engineering design tools must be able to correctly predict the in-depth temperature experienced by the internal structure of the

* Corresponding author at: I2M - Institute of Mechanical Engineering of Bordeaux: UMR CNRS 5295, University of Bordeaux, Arts et Métiers Institute of Technology, Hesam Université, Bordeaux INP, INRAE, 33400, Talence, France.
E-mail address: scandellihermes@gmail.com (H. Scandelli).

https://doi.org/10.1016/j.ast.2023.108297

Nomenclature

Latin Letters

$\underline{\underline{K}}$	permeability tensor ..... $[m^2]$
$\underline{\underline{k}}_{eff}$	effective thermal conductivity tensor .... $[Wm^{-1}K^{-1}]$
$\boldsymbol{x}$	position vector ..... $[m]$
$\boldsymbol{v}$	macro-scale velocity ..... $[m\,s^{-1}]$
$\mathcal{A}$	Arrhenius law pre-exponential factor
A	generic element/species
C_m	mass transfer coefficient ..... $[kgm^{-2}s^{-1}]$
c_p	specific heat ..... $[Jkg^{-1}K^{-1}]$
d_p	mean pore diameter ..... $[m]$
$\mathcal{E}$	Arrhenius law activation energy ..... $[Jmol^{-1}]$
e	specific energy ..... $[J\,kg^{-1}]$
$\mathcal{F}$	effective diffusion flux ..... $[kgm^{-2}s^{-1}]$
h	specific absolute enthalpy ..... $[Jkg^{-1}]$
h_v	volumetric heat transfer coefficient ..... $[Wm^{-3}K^{-1}]$
$\mathcal{M}$	molar mass ..... $[kgmol^{-1}]$
m, n	Arrhenius law parameters
N_g	number of gaseous species
$N_{p,i}$	number of sub-phases in the solid phase i
N_s	number of solid phases
$\mathcal{P}_i, \mathcal{P}_{i,j}$	solid phase i and sub-phase j of solid phase i
p	macro-scale pressure ..... $[Pa]$
Q	effective diffusion heat flux ..... $[Jm^{-2}s^{-1}]$
R	specific perfect gas constant ..... $[Jmol^{-1}K^{-1}]$
T	macro-scale temperature ..... $[K]$
t	time ..... $[s]$
y, z	species, element mass fractions

Greek Letters

$\underline{\underline{\beta}}$	Klinkenberg correction tensor ..... $[Pa]$
Δ	relative difference
ϵ	volume fraction
μ	dynamic viscosity ..... $[Pas]$
ν	stoichiometric coefficient
π_k	pyrolysis mass production rate of element/species ..... k $[kgm^{-3}s^{-1}]$
Π	global mass production rate of the pyrolysis reactions ..... $[kgm^{-3}s^{-1}]$
ρ	macro-scale density ..... $[kgm^{-3}]$
$\chi_{i,j}$	advancement of the pyrolysis reaction of sub-phase j within phase i

Subscripts and Superscripts

0	initial time
c, v	char and virgin
eff	effective
g	gas
i, j, k	indexes used in the sum operators
s	solid
tot	total
w	wall

Adimensional Groups

Pe	thermal Peclet number

Acronyms

LTE	Local Thermal Equilibrium
$LTNE$	Local Thermal Non-Equilibrium
MSL	Mars Science Laboratory
$PATO$	Porous material Analysis Toolbox based on OpenFoam
REV	Representative Element Volume
$TACOT$	Theoretical Ablative Composite for Open Testing
TPS	Thermal Protection System

vehicle as well as the total recession of the material. As described above, an atmospheric entry involves a wide range of phenomena, which makes the development of these tools challenging. This leads to the introduction of assumptions into the design models in order to simplify the description. It is therefore important to check the accuracy of these assumptions in the assessment of the efficiency of the ablator, to avoid unnecessarily increasing the safety margin in the design process. In particular, one of the most common assumption is to consider Local Thermal Equilibrium (LTE) between the gas phase and the solid phase of porous ablative materials, meaning the gas temperature accommodates to the solid one within the pores. It follows that a single governing equation is used to model the conservation of energy. According to Puiroux et al. [7], this assumption can generically be considered true as long as the Peclet number for heat diffusion inside the pores is small ($Pe \ll 1$). In the case of entry flow conditions, the small pore size ($d_p < 100$ µm) and the slow pyrolysis gas flow ($v_g \sim 1\ m/s$) ensure the condition to be true. However, the validity of this analysis may fall under some circumstances. The thermal Peclet number may become large due to high pyrolysis gas velocities, or additional physical phenomena not considered in the non-dimensional number may turn out to be non-negligible, such as strong variations of enthalpy due to chemical reactions. Under these circumstances, a Local Thermal Non-Equilibrium (LTNE) model, i.e. two energy conservation equations, would be necessary to accurately characterize the temperature of the gas. The importance of this aspect lies in the fact that the chemical reactions taking place in the mixture are strongly affected by the temperature of the gas. The use of LTE models, when inappropriate, may lead to an incorrect description of the gas phase.

The objective of this study is two-fold. First, a detailed two temperature material response model for reactive porous materials is presented. This model has been implemented and made available in the Porous material Analysis Toolbox based on OpenFOAM (PATO). Its numerical description is presented in Section 2. Secondly, in Section 3, the model is applied to the Theoretical Ablative Composite for Open Testing (TACOT) in a wide range of conditions to assess the true range of validity of the thermal equilibrium hypothesis. Simulations are carried out on the Stardust and Mars Science Laboratory (MSL) atmospheric entries with both chemical equilibrium and non-equilibrium conditions. For the latter case, the nonequilibrium mechanism based on an experimental campaign and proposed by April and Pike [8] is adopted. Finally, conclusions are drawn in Section 4.

2. Numerical model

The material response code, PATO, has been implemented and validated over the last decade [9–11]. In what follows, a short review of its main assumptions and governing equations is presented. We invite the reader to refer to the cited articles for more details.

2.1. Main assumption

The model provides the numerical description of the interaction between a multi-phase reactive material (N_s solid phases) with a

multi-species reactive gas mixture (N_g gaseous elements/species). The reactive material is assumed to be rigid and the gas phase to be a mixture of compressible and perfect gaseous elements/species. The gas mixture is constrained to the creeping regime. Any liquid phase present in the ablative material (such as water) is modelled as a solid static phase. The numerical description is carried out at the macro-scale. The governing equations are derived from upscaling theories [12–14], relying on the existence of a Representative Elementary Volume (REV) of the domain and on the assumption of scales separation. The specific choice of the upscaling theory is not critical, as all approaches lead to equivalent results, provided the same physical hypotheses and level of mathematical approximations [15]. Second order couplings, such as dispersion, are neglected. As the entire section is aimed at the macro-scale, unmarked notations are employed to address to intrinsic phase variables [11].

2.2. Pyrolysis

N_s solid phases compose the material. For example, in TACOT the main components are the carbon fiber preform and the phenolic resin, which are modelled as two phases. Each solid phase, $\mathcal{P}_i$, may decompose following multiple pyrolysis kinetics. We deal with this aspect by splitting each phase i into $N_{p,i}$ sub-phases. A generic sub-phase $\mathcal{P}_{i,j}$ undergoes a determined kinetic mechanism which results in the production of species, or element, A_k according to the stoichiometric coefficients $\nu_{i,j,k}$

$$\mathcal{P}_{i,j} \longrightarrow \sum_{k=1}^{N_g} \nu_{i,j,k} A_k \tag{1}$$

The Arrhenius model is adopted to model the pyrolysis reactions. This leads to the definition of the advancement of the pyrolysis reaction $\chi_{i,j}$ of sub-phase j within phase i as follows

$$\partial_t \chi_{i,j} = (1-\chi_{i,j})^{m_{i,j}} T_s^{n_{i,j}} \mathcal{A}_{i,j}\, exp\Big(-\frac{\mathcal{E}_{i,j}}{R\, T_s}\Big) \tag{2}$$

where m and n are the Arrhenius law parameters, $\mathcal{A}$ is the Arrhenius law pre-exponential factor, $\mathcal{E}$ represents the Arrhenius law activation energy, R stands for the perfect gas constant, and T_s indicates the temperature of the solid. By summing the productions of the N_s solid phases it is possible to derive the total production rate π of species/element k

$$\pi_k = \sum_{i=1}^{N_s} \sum_{j=1}^{N_{p,i}} \nu_{i,j,k}\, \epsilon_{i,0}\, \rho_{i,0}\, y_{i,j}\, \partial_t \chi_{i,j} \tag{3}$$

where $\epsilon_{i,0}$, $\rho_{i,0}$, and $y_{i,j}$, are respectively the initial (at t=0) volume fraction of phase i, intrinsic density of phase i, and mass fraction of sub-phase j within phase i. The overall pyrolysis-gas production rate Π is evaluated by summing over the elements and species in the mixture

$$\Pi = \sum_{k=1}^{N_g} \pi_k \tag{4}$$

2.3. Mass conservation

Each solid phase, each species/element, and the gas mixture are characterized by a mass conservation equation. No heterogeneous reactions are considered.

For a generic solid phases i, the equation reads

$$\partial_t(\epsilon_i \rho_i) = -\pi_i \tag{5}$$

where t is the time and the subscript 0 stands for the initial time ($t=0$).

Depending on the chemical model used in the gas phase, elements or species are considered (elements for equilibrium or species for finite-rate chemistry). In case of chemical equilibrium the conservation equation for a generic element with mass fraction z_k reads

$$\partial_t(\epsilon_g \rho_g z_k) + \partial_{\boldsymbol{x}} \cdot (\epsilon_g \rho_g z_k \boldsymbol{v_g}) + \partial_{\boldsymbol{x}} \cdot \boldsymbol{\mathcal{F}}_k = \pi_k \tag{6}$$

In case of finite rate chemistry, the conservation equation for a generic species with mass fraction y_i reads

$$\partial_t(\epsilon_g \rho_g y_i) + \partial_{\boldsymbol{x}} \cdot (\epsilon_g \rho_g y_i \boldsymbol{v_g}) + \partial_{\boldsymbol{x}} \cdot \boldsymbol{\mathcal{F}}_i = \pi_i \tag{7}$$

where $\mathcal{M}_g$ is the molar mass of the gas mixture and $\boldsymbol{\mathcal{F}}_i$ and $\boldsymbol{\mathcal{F}}_k$ [11] are the effective multicomponent diffusion mass fluxes of the i-th species and k-th element. Mutation++ [16,17], is used as a third party library to compute all thermodynamics and transport properties.

For the gas mixture, the mass conservation accounts for the pyrolysis production rate Π

$$\partial_t(\epsilon_g \rho_g) + \partial_{\boldsymbol{x}} \cdot (\epsilon_g \rho_g \boldsymbol{v_g}) = -\sum_{i=1}^{N_s} \partial_t(\epsilon_i \rho_i) = \Pi \tag{8}$$

2.4. Momentum conservation

The average gas velocity is obtained from the resolution of Darcy's law [18]

$$\boldsymbol{v_g} = -\frac{1}{\epsilon_g}\Big[\frac{1}{\mu_g}\underline{\underline{K}}\Big(1+\frac{1}{p_g}\underline{\underline{\beta}}\Big)\Big] \cdot \partial_{\boldsymbol{x}} p_g \tag{9}$$

where p_g is the gas pressure, $\underline{\underline{K}}$ is the permeability tensor, and $\underline{\underline{\beta}}$ the Klinkenberg correction introduced to account for slip effects (at the pore scale) when the Knudsen number is not very small. This expression for the gas velocity vector can be substituted back into the gas mass conservation law, Eq. (8). Assuming a mixture of perfect gases, the following equation in pressure is found

$$\partial_t\Big(\frac{\epsilon_g \mathcal{M}_g}{R T_g} p_g\Big) - \partial_{\boldsymbol{x}} \cdot \Big[\frac{\epsilon_g \mathcal{M}_g}{R T_g}\frac{1}{\mu_g}\underline{\underline{K}}\Big(1+\frac{1}{p_g}\underline{\underline{\beta}}\Big) \cdot \partial_{\boldsymbol{x}} p_g\Big] = \Pi + \Omega_h \tag{10}$$

where μ_g is the dynamic viscosity of the gas mixture.

2.5. Energy conservation

Under the assumption of LTE, the temperature of the gas mixture accommodates to the one of the solid: $T_s = T_g = T$. A single conservation equation is then considered [11]

$$\partial_t(\rho_{\text{tot}} e_{\text{tot}}) + \partial_{\boldsymbol{x}} \cdot (\epsilon_g \rho_g h_g \boldsymbol{v}_g) = \partial_{\boldsymbol{x}} \cdot \sum_{k=1}^{N_g} \boldsymbol{\mathcal{Q}}_k + \partial_{\boldsymbol{x}} \cdot \Big(\underline{\underline{k}}_{\text{eff}} \cdot \partial_{\boldsymbol{x}} T\Big) \tag{11}$$

where the subscript tot stands for total, e, h, and T denote respectively the internal energy, the absolute enthalpy, and the temperature, $\boldsymbol{\mathcal{Q}}_k$ is the heat transport by effective diffusion of the species, and $\underline{\underline{k}}_{\text{eff}}$ represents the effective thermal conductivity tensor. The terms on the left hand-side of the equation are the ones of accumulation and advection. While, on the right hand-side there are the terms of diffusion of the pyrolysis gases and the conduction flux. The conduction flux is described by Fourier's law

Table 1
Pyrolysis balance equations and kinetic parameters for the phenolic matrix in TACOT.

j	Pyrolyis of phenolic matrix	Peak (K)	$\mathcal{A}_{2,j}$ (s^{-1})	$\mathcal{E}_{2,j}$ (J/mol)	$m_{2,j}$	$n_{2,j}$
1	$\mathcal{P}_{2,1} \longrightarrow H_2O$	373	$8.56 \cdot 10^3$	$7.12 \cdot 10^4$	3	0
2	$\mathcal{P}_{2,2} \longrightarrow 0.69H_2O + 0.01C_6H_6 + 0.01C_7H_8 + 0.23C_6H_6O$	773	$8.56 \cdot 10^3$	$7.12 \cdot 10^4$	3	0
3	$\mathcal{P}_{2,3} \longrightarrow 0.09CO_2 + 0.33CO + 0.58CH_4$	873	$4.98 \cdot 10^8$	$1.70 \cdot 10^5$	3	0
4	$\mathcal{P}_{2,4} \longrightarrow H_2$	1073	$4.98 \cdot 10^8$	$1.70 \cdot 10^5$	3	0

where the effective conductivity tensor accounts for conduction in the gas and solid phases and radiative heat transfer within the pores [10,19].

Eq. (11) can be further developed by expressing the total storage internal energy ($\rho_{\text{tot}}\, e_{\text{tot}}$) as the sum of the energy of its phases

$$\rho_{\text{tot}} e_{\text{tot}} = \epsilon_g \rho_g e_g + \sum_{i=1}^{N_s} \epsilon_i \rho_i h_i \tag{12}$$

By substituting this term back in Eq. (11) and by performing the time derivatives, the energy conservation equation takes its final form

$$\begin{aligned}
&\sum_{i=1}^{N_s} \epsilon_i \rho_i c_{p,i} \partial_t T + \epsilon_g \rho_g c_{p,g} \partial_t T \\
&= \partial_{\boldsymbol{x}} \cdot \left(\underline{\underline{k}}_{\text{eff}} \cdot \partial_{\boldsymbol{x}} T \right) - \sum_{i=1}^{N_s} h_i \partial_t (\epsilon_i \rho_i) - \sum_{j=1}^{N_g} h_j \partial_t (\epsilon_g \rho_g y_j) \\
&+ \partial_t (\epsilon_g p_g) - \partial_{\boldsymbol{x}} \cdot (\epsilon_g \rho_g h_g \boldsymbol{v}_g) + \partial_{\boldsymbol{x}} \cdot \sum_{k=1}^{N_g} \boldsymbol{\mathcal{Q}}_k
\end{aligned} \tag{13}$$

where c_p is the specific heat. All the accumulation terms are gathered on the left hand-side of the equation. Whereas, on the right hand-side it is possible to find (in order) the terms related to conduction, pyrolysis, pressure, advection and species diffusion.

Under the assumption of LTNE, two energy conservation equations are needed to describe the solid and gas phases. The two equations are

$$\begin{aligned}
&\sum_{i=1}^{N_s} \epsilon_i \rho_i c_{p,i} \partial_t T_s + \sum_{i=1}^{N_s} h_i \partial_t (\epsilon_i \rho_i) \\
&= \partial_{\boldsymbol{x}} \cdot \left(\underline{\underline{k}}_{\text{eff},s} \cdot \partial_{\boldsymbol{x}} T_s \right) + h_v \left(T_g - T_s \right)
\end{aligned} \tag{14}$$

and

$$\begin{aligned}
&\epsilon_g \rho_g c_{p,g} \partial_t T_g + \sum_{j=1}^{N_g} h_j \partial_t (\epsilon_g \rho_g y_j) - \partial_t (\epsilon_g p_g) \\
&= -\partial_{\boldsymbol{x}} \cdot \left(\epsilon_g \rho_g \boldsymbol{v}_g h_g \right) + \partial_{\boldsymbol{x}} \cdot \left(\underline{\underline{k}}_{\text{eff},g} \cdot \partial_{\boldsymbol{x}} T_g \right) \\
&+ \partial_{\boldsymbol{x}} \cdot \sum_{k=1}^{N_g} \boldsymbol{\mathcal{Q}}_k + h_v \left(T_s - T_g \right)
\end{aligned} \tag{15}$$

where h_v is the volumetric heat transfer coefficient that identifies the heat exchanged by the two phases. It should be mentioned, if summing the two LTNE equations (Eq. (14) and Eq. (15)), the LTE equation (Eq. (13) is obtained.

3. Application of the model to the ablation cases

In this section, the numerical model is applied in order to assess the validity of the thermal equilibrium hypothesis for atmospheric entry applications. Two different ablation cases are considered: Stardust and MSL missions. A subsection is dedicated to each of them. The same ablative material, TACOT, is considered for all cases. This theoretical material is characterized by a composition and properties that are comparable to NASA's Phenolic Impregnated Carbon Ablator. In volume, TACOT is made of 10% of carbon fibers (phase-1) and 10% of phenolic resin (phase-2), hence $N_s = 2$. It is 80% porous (phase-0: gas). During the thermal degradation process, the carbon fibers phase does not decompose, while the phenolic resin undergoes several parallel pyrolysis mechanisms, as showed in Table 1. 1D Simulations have been carried out on uniform meshes. The thickness of the geometry is specified in each subsection. A convective thermal boundary condition (Bprime [20]) involving the resolution of the mass and energy balances at the surface [9] is enforced to the surface with the external environment; an adiabatic condition characterizes the bottom boundary. A 600-cells mesh has been adopted following a mesh convergence analysis. To account for the material response, that is for the shape changes due to surface recession, PATO adopts an unstructured moving mesh technique.

Table 2
Modified April mechanism [8] considered for the chemical non-equilibrium analysis.

	Reaction Formula	$\mathcal{A}$ (s^{-1})	$\mathcal{E}$ (J/mol)
1	$CH_4 \longrightarrow 0.5\ H_2 + 0.5\ C_2H_6$	$7.6\ 10^{14}$	397480
2	$C_2H_6 \longrightarrow H_2 + C_2H_4$	$3.1\ 10^{14}$	292880
3	$C_2H_4 \longrightarrow C_2H_2 + H_2$	$2.6\ 10^{8}$	167360
4	$C_2H_2 \longrightarrow 2C + H_2$	$2.1\ 10^{10}$	167805
5	$C + 2H_2 \longrightarrow CH_4$	$2.0\ 10^{9}$	71128
6	$C_6H_5OH + H_2 \longrightarrow H_2O + C_6H_6$	$2.0\ 10^{13}$	188280
7	$C_6H_6 \longrightarrow 3\ C_2H_2$	$1.4\ 10^{9}$	246440
8	$C + H_2O \longrightarrow CO + H_2$	$1.2\ 10^{12}$	343088
9	$CO + H_2O \longrightarrow H_2 + CO_2$	$1.0\ 10^{10}$	125520
10	$C + CO \longrightarrow 2\ CO$	$1.0\ 10^{6}$	209200
11	$2\ CO \longrightarrow C + CO$	$1.0\ 10^{-9}$	255224

For each case, both the LTE (Eq. (13)) and the LTNE (Eqs. (14) and (15)) models are applied. Results are then compared and commented. The comparison is made in terms of temperature evolution and species concentration (non-equilibrium) within the material, pyrolysis gas blowing rate at the surface, wall recession due to pyrolysis ablation, and identification of the pyrolysis zone. The latter is defined as the intermediate region between two thresholds in terms of the density: virgin 98% and char 2%, defined as $\rho_v(98\%) = \rho_c + 0.98(\rho_v - \rho_c)$ and $\rho_c(2\%) = \rho_c + 0.02(\rho_v - \rho_c)$. The relative difference, Δ between the results is defined as follows

$$\Delta = \frac{\rho_v(98\%)_{1T} - \rho_v(98\%)_{2T}}{\rho_v(98\%)_{1T}}\ 100 \tag{16}$$

where the quantity $\rho_v(98\%)$ is taken as example.

In order to apply the LTNE model, it is necessary to quantify the volumetric heat transfer coefficient between the gas phase and the TACOT material. Its value has been set equal to $h_v = 10^9\ Wm^{-3}K^{-1}$, after experimental characterization [21].

For the chemical non-equilibrium analysis, a modified April mechanism [8] has been considered for the composition of the gas mixture. This mechanism is reported in Table 2.

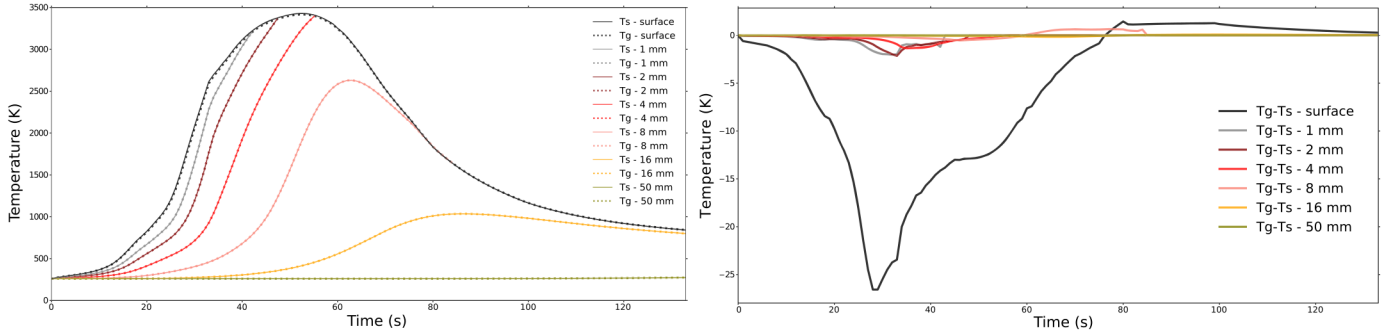

Fig. 1. Stardust case. Thermocouple data are reported on the left figure and temperature difference on the right one.

Table 3
Stardust case. Partial summary of the environment properties. Input data are the wall pressure and enthalpy, p_w, h_w and the mass transfer coefficient C_m.

t (s)	p_w (Pa)	C_m $(kg/m^2/s)$	h_w (J/kg)
0	1.5	0.00005	77926960
1	1.8	0.00006	77984280
2	2.1	0.00007	78040736
3	2.4	0.00008	78095240
4	2.6	0.00009	78146168
..	..	..	..
50	19142.319	0.17378	61280148
51	21350.19075	0.18082	59093460
52	23558.0625	0.18786	56748968
..	..	..	..
131	2144.746275	0.01705	95178
132	2067.8406	0.01644	89990
133	2067.8406	0.01582	84957

3.1. Stardust ablation case

The Stardust mission was a 390-kilogram robotic space probe launched by NASA on 7 February 1999. Its primary mission was to collect dust samples from the coma of the comet Wild 2, as well as cosmic dust samples, and return these to Earth for analysis. It was the first sample-return mission of its kind. The primary mission was successfully completed on 15 January 2006, when the sample space probe returned to Earth.

The TPS is modelled as a 1D material composed of three layers: 5.8 cm of TACOT material, 0.14 cm of adhesive film (HT-424), and 1.27 cm of aluminium 2024 [22]. An overview of the input data for the convective boundary condition is given in Table 3. Standard air is considered for the initial gas composition of the material and for the element composition at the boundary.

3.1.1. Chemical equilibrium

Results of the thermocouple and temperature difference are showed in Fig. 1 Without any abrupt change of condition, the gas temperature tends to be closer to that of the solid. Referring to the figure on the right, it can be seen that at most, the difference between the two predictions is about 25 K. Considering that the temperatures are about 3000 K, the 25 K difference (less than 1%) can be considered negligible. In fact, in the figure on the left, the temperature curves of the gas and the solid are superimposed at each position. This aspect is also reflected in the comparison of other quantities of interest. This is represented in Fig. 2, where the maximum relative difference, $\Delta = 0.2\%$ is related to the prediction of the location of the virgin front.

3.1.2. Chemical non-equilibrium

The species distribution within the material at time $t = 40\,s$ is reported in Fig. 3 It can be observed that the use of LTE or LTNE strongly influences the species distribution. In particular, CO, H_2, CH_4, and CO_2 are the species that undergo a higher difference in the predictions. The difference concerns both the evolution of the mass fractions in the material and at the interface with the external environment. It follows that, depending on the model, the boundary layer will be characterized by a different composition, hence different properties.

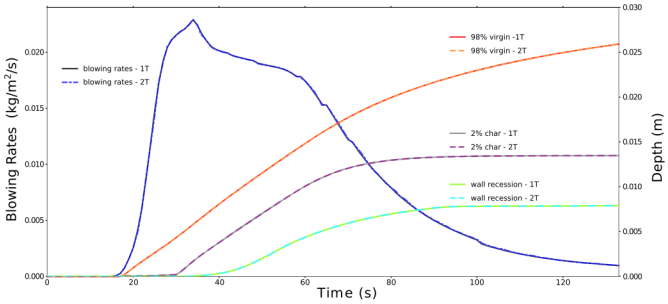

Fig. 2. Stardust case. Blowing rates, pyrolysis zone, and wall recession.

3.2. MSL ablation case

The Mars Science Laboratory mission was a robotic space probe mission to Mars launched by NASA on November 26, 2011. It successfully landed Curiosity, a Mars rover, in Gale Crater on August 6, 2012. The overall objectives include investigating Mars' habitability, studying its climate and geology, and collecting data for a human mission to Mars.

The depth of the ablative material is of 4.385 *cm* [20]. The Mars atmosphere is considered for the initial gas composition of the material and for the composition of the elements in the boundary layer. The input data for the convective boundary layer are taken from the study by Meurisse et al., 2018 [20], where 11 discrete times along the MSL trajectory are considered: 48.4, 59.1, 64.4, 69.6, 71.5, 73.9, 76.2, 80.5, 84.4, 87.5 and 100.5 *s*. A linear variation of the conditions is assumed in the intermediate intervals.

3.2.1. Chemical equilibrium

The thermocouple and temperature difference results are showed in Fig. 4. A difference of 40 *K* is reached at the beginning of the simulation between the two temperatures due to the initial sharp change of condition. After the first few seconds in which the value remains constant, the difference gradually decreases to 3 *K* at 100.5 *s*. Nevertheless, as can be seen in Fig. 5, this small difference in temperature does not lead to any discrepancy on any other quantity of interest. The maximum relative error is still provided by the prediction of the virgin front location with a value of 0.2%.

3.2.2. Chemical non-equilibrium

The species distribution within the material at time $t = 70\,s$ is reported in Fig. 6. The figures show again a clear difference be-

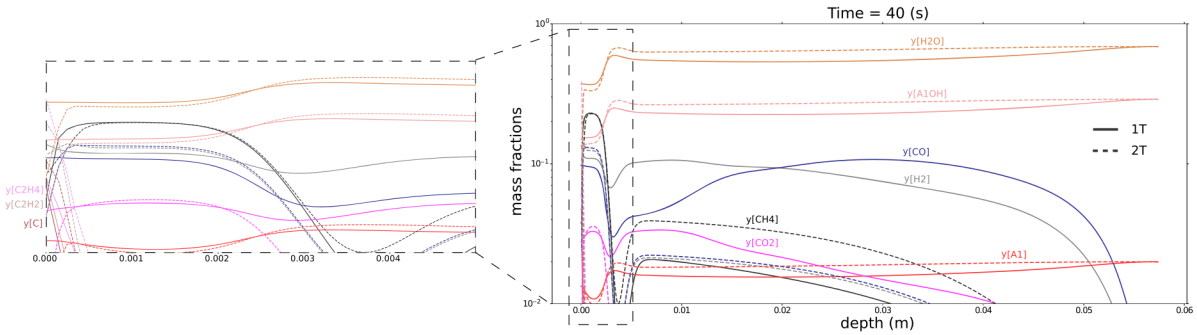

Fig. 3. Stardust case. Species distribution within the material at time $t = 40\,s$. At the left: a zoom of the mass fractions near the surface with the external environment.

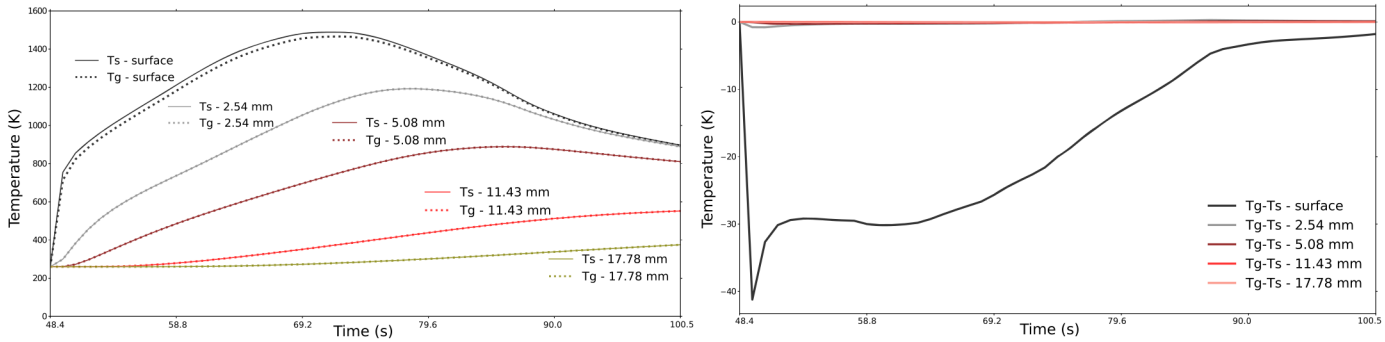

Fig. 4. MSL case. Thermocouple data are reported on the left figure and temperature difference on the right one.

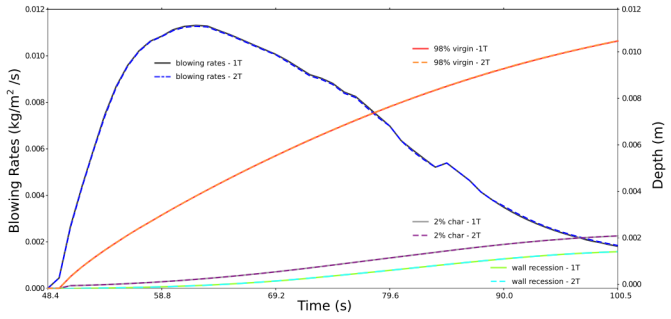

Fig. 5. MSL case. Blowing rates, pyrolysis zone, and wall recession.

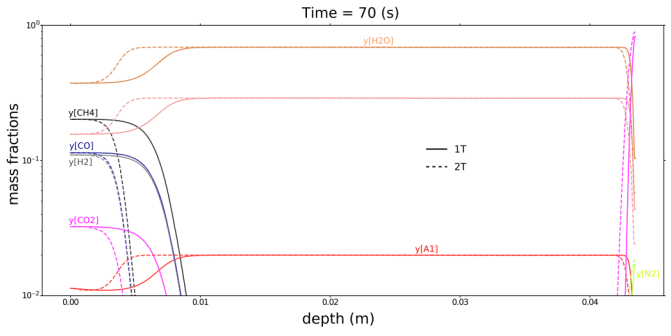

Fig. 6. Stardust case. Species distribution within the material at time $t = 21s$.

tween the two models. However, due to the lower temperatures reached, the difference is less marked than in the Stardust case. The species difference concerns only the internal part of the material, and not the interface. The composition of the boundary layer between the two models remains unaltered.

4. Conclusions and perspectives

This study investigates the validity of the local thermal equilibrium assumption for ablative material responses. To this end, a two-temperature model has been implemented and integrated in the Porous material Analysis Toolbox based on OpenFOAM (PATO). This toolbox has been then used to simulate the pyrolysis of the Theoretical Ablative Composite for Open Testing (TACOT) in a wide range of conditions to assess the true range of validity of the thermal equilibrium hypothesis. 1D simulations are performed on the Stardust and Mars Science Laboratory atmospheric entry missions. Both Local Thermal Equilibrium (LTE) and Local Thermal Non-Equilibrium (LTNE) energy models have been adopted. The comparison between the two models has been carried out by monitoring the temperature evolution and species concentration (non-equilibrium) inside the material, the pyrolysis gas blowing rate, the pyrolysis zone, and the wall recession due to ablation. Results show that the gas temperature does not perfectly match that of the solid at the surface, especially when a sudden change in conditions occurs. Nevertheless, the temperature difference does not lead to a significant deviation in the monitored quantities (the maximum relative difference in the results has been found to be about $\Delta = 1.4\%$) under chemical equilibrium assumption. The relative difference values are possible sources of uncertainty to include in the design analysis. The same conclusion does not hold for the case of chemical non-equilibrium. In this case, especially in the Stardust case where higher temperatures are reached, the species distribution prediction is strongly influenced by the use of LTE or LTNE models. In particular, the difference concerns both the evolution of the mass fractions of the species in the material and at the interface with the external environment. It follows that, depending on the model, the boundary layer will be characterized by a different composition, hence different properties.

Results obtained in this study must be considered with caution. As the main purpose of the work is to estimate possible differences resulting from the use of LTE or LTNE models, no effort has been directed towards the description of chemical mechanisms.

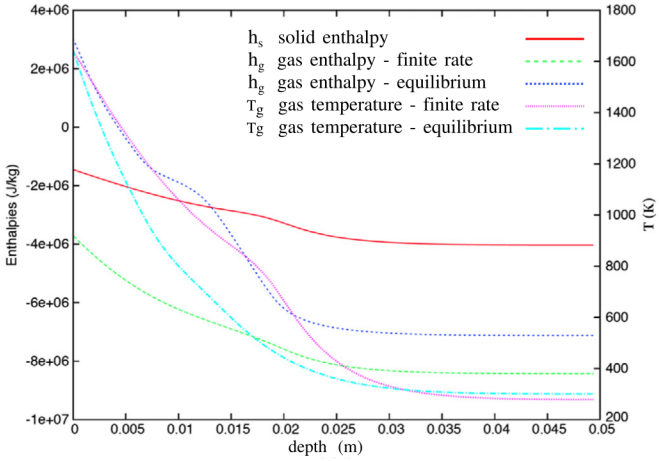

Fig. 7. Test case #1. Comparison of the temperature and enthalpy profiles.

The April mechanism has been employed, despite knowing its inaccuracy. In the perspective of a more realistic modelling, greater efforts must be placed on the description of the chemical mechanisms and in particular on the estimation of the enthalpy variations of individual reactions. An acknowledgement of this problem can be seen in Fig. 7, where the pyrolysis gas enthalpies profiles within the material, at equilibrium and finite rate, are reported for the ablative test case #1. It can be observed how the two are significantly different, thus underlining a fundamental problem in the treatment of the pyrolysis mechanism.

Declaration of competing interest

The authors declare the following financial interests/personal relationships which may be considered as potential competing interests: Scandelli Hermes reports financial support was provided by Arts et Métiers Sciences et Technologies. Scandelli Hermes reports a relationship with Arts et Métiers Sciences et Technologie that includes: employment and funding grants.

Data availability

Data will be made available on request.

Acknowledgements

The research of H.S. was sponsored by a PhD grant awarded by Arts et Métiers Institute of Technology.

References

[1] Michael J. Wright, Robin As Beck, Karl T. Edquist, David Driver, Steven A. Sepka, Eric M. Slimko, William H. Willcockson, Sizing and margins assessment of Mars science laboratory aeroshell thermal protection system, J. Spacecr. Rockets 51 (4) (2014) 1125–1138.
[2] Mairead Stackpoole, Steve Sepka, Ioana Cozmuta, Dean Kontinos, Post-flight evaluation of stardust sample return capsule forebody heatshield material, in: 46th AIAA Aerospace Sciences Meeting and Exhibit, 2008, p. 1202.
[3] Raffaele Savino, Mario De, Stefano Fumo, Diego Paterna, Michelangelo Serpico, Aerothermodynamic study of uhtc-based thermal protection systems, Aerosp. Sci. Technol. 9 (2) (2005) 151–160.
[4] Huy K. Tran, C. Johnson, D. Rasky, F. Hui, Ming-Ta Hsu, Timothy Chen, Y. Chen, Daniel Paragas, Loreen Kobayashi, Phenolic Impregnated Carbon Ablators Pica as Thermal Protection System for Discovery Missions, NASA TM-110440, NASA, Washington, DC, 1997.
[5] H. Ritter, P. Portela, K. Keller, J.M. Bouilly, S. Burnage, Development of a European ablative material for heatshields of sample return missions, in: 6th European Workshop on Thermal Protection Systems and Hot Structures, Stuttgart, Germany, vol. 99, 2009.
[6] Alexandre Martin, Iain D. Boyd, Modeling of heat transfer attenuation by ablative gases during the stardust reentry, J. Thermophys. Heat Transf. 29 (3) (2015) 450–466.
[7] N. Puiroux, Marc Prat, Michel Quintard, Non-equilibrium theories for macroscale heat transfer: ablative composite layer systems, Int. J. Therm. Sci. 43 (6) (2004) 541–554.
[8] Gary C. April, Ralph W. Pike, Eduardo G. Del Valle, Modeling reacting gas flow in the char layer of an ablator, AIAA J. 9 (6) (1971) 1113–1119.
[9] Jean Lachaud, Nagi N. Mansour, Porous-material analysis toolbox based on openfoam and applications, J. Thermophys. Heat Transf. 28 (2) (2014) 191–202.
[10] Jean Lachaud, Tom van Eekelen, James B. Scoggins, Thierry E. Magin, Nagi N. Mansour, Detailed chemical equilibrium model for porous ablative materials, Int. J. Heat Mass Transf. 90 (2015) 1034–1045.
[11] Jean Lachaud, James B. Scoggins, Thierry E. Magin, M.G. Meyer, Nagi N. Mansour, A generic local thermal equilibrium model for porous reactive materials submitted to high temperatures, Int. J. Heat Mass Transf. 108 (2017) 1406–1417.
[12] Gedeon Dagan, Shlomo P. Neuman, Subsurface Flow and Transport, International Hydrology Series, 1997.
[13] Stephen Whitaker, The Method of Volume Averaging, vol. 13, Springer Science & Business Media, 2013.
[14] E. Sanchez-Palencia, Homogenization method for the study of composite media, in: Asymptotic Analysis II, Springer, 1983, pp. 192–214.
[15] John H. Cushman, Lynn S. Bennethum, Bill X. Hu, A primer on upscaling tools for porous media, Adv. Water Resour. 25 (8–12) (2002) 1043–1067.
[16] James B. Scoggins, Thierry E. Magin, Development of mutation++: multicomponent thermodynamic and transport properties for ionized plasmas written in C++, in: 11th AIAA/ASME Joint Thermophysics and Heat Transfer Conference, 2014, p. 2966.
[17] James B. Scoggins, Thierry E. Magin, Gibbs function continuation for linearly constrained multiphase equilibria, Combust. Flame 162 (12) (2015) 4514–4522.
[18] Stephen Whitaker, Flow in porous media I: a theoretical derivation of Darcy's law, Transp. Porous Media 1 (1) (1986) 3–25.
[19] A.J. Van Eekelen, J. Lachaud, Numerical validation of an effective radiation heat transfer model for fiber preforms, J. Spacecr. Rockets 48 (3) (2011) 534–537.
[20] Jeremie Be Meurisse, Jean Lachaud, Francesco Panerai, Chun Tang, Nagi N. Mansour, Multidimensional material response simulations of a full-scale tiled ablative heatshield, Aerosp. Sci. Technol. 76 (2018) 497–511.
[21] Liu Shaolin, Ahmadi Azita, Lachaud Jean, Experimental investigation of heat transfer in calcarb: one or two temperature model?, in: 2nd International Conference on Flight Vehicles, Aerothermodynamics and Re-entry Missions Engineering (FAR), 2022.
[22] Kerry A. Trumble, Ioana Cozmuta, Steve Sepka, Peter Jenniskens, Michael Winter, Postflight aerothermal analysis of the stardust sample return capsule, J. Spacecr. Rockets 47 (5) (2010) 765–774.